FERMILAB-PUB-79-088-E

MSU-CSL-70
June, 1979

MULTIMUON FINAL STATES IN *MUON-NUCLEON SCATTERING AT 270 GeV*

D. Bauer, J. Kiley, R. Ball, C. Chang [(a)],
K. W. Chen, M. Ghods, S. Hansen [(b)],
A. Kotlewski [(c)], L. Litt [(c)], P. F. Schewe [(d)]
Michigan State University
East Lansing, Michigan 48824
and
A. Van Ginneken
Fermi National Accelerator Laboratory
Batavia, Illinois 60510

ABSTRACT

Data from a new muon-nucleon scattering experiment includes 513 events with more than one final state muon, of which 449 are dimuons and 64 are trimuons. Conventional hadronic and electromagnetic processes account for less than 15% of these events. Present calculations suggest that the majority of the dimuons result from the associated production and semi-leptonic decay of charmed mesons.

(Submited for Publication in Phys. Rev. Lett.)

Events with two (or more) final state muons have been observed in several experiments using muons[1], neutrinos[2], or hadrons[3] as incident particles. Interpretations of these events in the lepton scattering experiments have included such processes as the production (and semi-leptonic decay) of charmed mesons[4], heavy lepton production and decay[5], and more conventional hadronic and electromagnetic mechanisms[1]. This Letter describes the characteristics of a large sample of dimuon events from a new *muon scattering experiment. The acceptance improvements and increased* statistics of this data have reduced the uncertainty about the origin of these events.

The experimental apparatus (Fig. 1) consisted of four major parts: the beam, the target/calorimeter, the final state muon spectrometer and the triggering/veto counters. The Fermilab muon (μ^+) beam energy was 270 GeV (with a mean spread of 5 GeV) and the intensity within the beam telescope averaged 6×10^5 muons/spill with an almost equal number of halo muons outside of the beam. This halo was prevented from triggering the apparatus by a large bank of scintillation counters at the front of the target. The target/calorimeter consisted of 110 steel plates (each 4.8 cm thick) sandwiched with scintillation counters, giving a total length of 738 cm (4250 gm/cm^2). The calorimeter was used to determine the vertex position, hadron energy, and the number of muons entering and leaving the target. The final state muons were detected in a large-aperture magnetic spectrometer consisting of eight toroidal iron magnets, and nine wire spark chambers. The field-free region of the toroid holes was filled with lead-loaded concrete to stop penetrating hadrons. The momentum resolution

of the spectrometer, about 10% for fully-penetrating muons, increased to nearly 40% near the acceptance edges. The front of the spectrometer was equipped with two small proportional chambers to improve multi-track recognition, and two large slabs of steel (770 gm/cm^2) to shield the spark chambers from hadrons. Three banks of scintillation counters were placed within the spectrometer for triggering purposes and three circular veto counters, centered on the magnet holes, rejected events with penetrating particles at small angles.

Multimuon event finding began with the reconstruction of all spectrometer tracks for those events with a single beam muon. The distance of closest approach of the incident and scattered muons (DMIN) defined the event vertex along the beam axis (ZMIN). Requiring DMIN < 10 cm and ZMIN to be within 80 cm of the target effectively eliminated halo contamination. All reconstructed tracks were required to penetrate at least one magnet, imposing a minimum energy of 5 GeV (at the end of the target) on all muons. Events with more than one reconstructed track (about 2% of the total of 8.2 x 10^5 events) were visually scanned to determine if the tracks constituted a genuine multimuon. Candidates had to have two (or more) good spectrometer tracks coming to a vertex within the target, clear timing information from the trigger counters, and a multi-particle signal from the calorimeter. The resulting 600 events were re-scanned to insure correct identification of the tracks. Reconstruction losses (mainly due to spark chamber inefficiency) were estimated by scanning 1.5% of the raw data triggers. Multiple scans of most of the multi-track events determined the scanning losses. These checks established an overall finding efficiency of 70 (± 8)% for dimuons and 89 (± 8)% for

trimuons.

The multimuon acceptance of the experiment is complicated by the trigger/veto requirements, the beam spread, and track curvature in the magnets. It is also model-dependent due to produced particle correlations. Nevertheless, the major acceptance features can be adequately described by simple energy and angle cuts on the final state muons. Defining the leading (μ_1+) and produced ($\mu_2\pm$) muons by their momenta ($p_1 > p_2$) gives minimum energies of 9 (18) GeV for p_1 and 5 (13) GeV for p_2, corresponding to an interaction at the downstream (upstream) end of the target. Similarly, the angular cut ranges are 13 (8) mrad < θ_1 < 74 (45) mrad and 26 (11) mrad < θ_2 < 144 (64) mrad.

From the sample of 1.1 x 10^{10} incident muons, we have found 449 dimuons and 64 trimuons. Application of the finding efficiency corrections increases these numbers to 644 (± 55) dimuons and 72 (± 6) trimuons. Subjecting the leading particles of multimuon events to the more stringent cuts applied to the deep-inelastic muon sample of 3.9 x 10^5 events gives rates per deep-inelastic scatter of 6.3 (± .6) x 10^{-4} dimuons and 4.1 (± .4) x 10^{-5} trimuons, uncorrected for the produced muon acceptance.

Full kinematic information is available for 412 dimuon events, of which 298 have particles with opposite charges (OSP), and 114 have particles of the same charge (SSP). Note that the definition of the leading and produced muons mis-identifies 26 OSP events where $p_2^- > p_1^+$. Fig. 2 compares the characteristics of deep-inelastic scattered muons and leading particles from dimuons. The leading muons prefer lower x and higher W (and y) regions, partly due to the acceptance difference. The sharp

rise (and fall) in W seems to be primarily an acceptance effect, which tends to mask any actual threshold.

To test various interpretations of multimuons, a Monte Carlo procedure has been developed which can accept any theoretical model and predict the rates and kinematic distributions expected within this experiment. The full incident beam distribution is used and all final state muons are traced through the spectrometer accounting for energy loss, multiple scattering, and momentum resolution, as well as trigger and veto requirements. Weighted histograms of relevant kinematic variables are then produced, with the weight being a product of the model cross section and the apparatus acceptance. This method has been used to examine several processes, including charm production, dimuons from π/K decay, and elastic Bethe-Heitler trident production. Dimuons arising from the decay of one of the pions (kaons) in the hadron shower, or from prompt muon production, have been calculated in the same manner as in the previous experiment.[7] The number of dimuons predicted from these processes is less than 15% of the observed sample. Dimuon and trimuon rates from elastic Bethe-Heitler muon-trident production were calculated using the computer code of Brodsky and Ting to give the differential cross section.[8] This process can account for only about 12 dimuons and 8 trimuons, because the veto severely biases the trigger against such low angle processes. Other potential backgrounds, including vector meson production, inelastic trident production and hadronic final state interactions have not yet been evaluated, but the calculations of Barger et al.[9] suggest that none of these processes can account for more than a small fraction of the observed dimuons.

The charm model (similar to that of Bletzacker and Nieh[4] for associated $D\bar{D}$ production) contains three free parameters governing the normalization

and the longitudinal and transverse momentum distributions.[6] With data at a single incident energy, the normalization is not determined and only kinematic shapes are obtained.

Fig. 3 shows some of the dimuon kinematic distributions, with curves from the π/K and trident backgrounds. The distributions in $\Delta\theta$ and $M_{\mu\mu}$ are rather smooth, with no striking features. The pronounced peaking at 180^0 in $\Delta\phi$ seems to occur in all of the calculated processes and represents the tendency of the produced muons to lie along the virtual photon direction, "back-to-back" with the scattered muon. The inelasticity favors the production of particles at the hadronic vertex and is inconsistent with the background shapes. The dimuon produced particle energy and transverse momentum (relative to the virtual photon direction) are shown in Fig. 4 with curves for the background processes and the charm model. The background shapes and rates cannot explain more than 15% of the data. The charm calculation fits reasonably well at low transverse momenta, but falls off somewhat faster than the data. This may indicate some problems in the model used, although an independent calculation[9] suggests the same trend.

In summary, the majority of dimuon events in muon scattering appear to result from the associated production and semi-leptonic decay of charmed mesons. Conventional hadronic and electromagnetic backgrounds are suppressed by the veto and cannot account for more than 15% of the dimuon sample. The small excess of high $p_\perp$ events may signal the need for more refined model calculations, although new processes are not ruled out.

We acknowledge the support of the Fermilab staff. We also thank the entire group of scanners (especially M. Brake, M. Kaianski, and B. Spero) for their perseverance in the event finding process. This research was

supported in part by the National Science Foundation under Grant No. 23365 and by the U.S. Department of Energy under Contract No. E(11-1)-1764.

(a) Present address: National Central University, Chung-Li, Taiwan, Republic of China

(b) Present address: Fermi National Accelerator Laboratory, Batavia, Illinois 60510.

(c) Present address: University of Miami School of Medicine, Biscayne Annex, Miami, Florida 33152.

(d) Present address: Brookhaven National Laboratory, Upton, New York 11973

References

1. C. Chang et al., Phys. Rev. Lett. 39, 519 (1977).
2. e.g., A. Benvenuti et al., Phys. Rev. Lett. 41, 725 (1978); 41, 1204 (1978).
3. K. J. Anderson et al., Phys. Rev. Lett. 42, 944 (1979).
4. F. Bletzacker et al., Phys. Rev. Lett. 37, 1316 (1976).
5. Carl H. Albright, Phys. Rev. D 12, 1319 (1975).
6. K. W. Chen and A. Van Ginneken, Phys. Rev. Lett. 40, 1417 (1978).
7. K. W. Chen in Proceedings of the International Conference on New Particles With New Quantum Numbers, Univ. of Wisconsin, Madison, 1976.
8. S. Brodsky and S. C. C. Ting, Phys. Rev. 145, 1018 (1966).
9. V. Barger et al., "Multimuon Production by Muons", Wisconsin Preprint COO-881-83, Phys. Rev. (in press); "Charm Muoproduction With A Small-Angle Veto", Wisconsin Preprint COO-881-100.

FIGURE CAPTIONS

Fig. 1. Layout of E319 apparatus. HV denotes the halo-veto scintillation counters, BEAM PCS and HPCS are proportional chambers, HS1 and HS2 are steel hadron shields, WSC1-9 are wire spark chambers, M1-M8 are iron toroidal magnets, SA, SB, and SC are trigger counter banks, and BV1-3 are beam-veto counters. A dimuon event (OSP) and its high-gain ADC readout are displayed.

Fig. 2. Histograms of the 4-momentum transfer squared Q^2 [$=4E_0E_1 \sin^2(\theta_1/2)$, where E_0=beam energy, E_1=scattered muon energy, and θ_1=scattered muon polar angle relative to the beam], Bjorken X [$=Q^2/2M\nu$, where $\nu=E_0 - E_1$ and M=nucleon mass], final state hadron energy W [$=(2M\nu + M^2 - Q^2)^{1/2}$], and fractional energy of the virtual photon Y [$=\nu/E_0$]. The solid (upper) histogram represents deep-inelastic single muons and refers to the arbitrary left scale. The dashed histogram shows leading muons from the full dimuon sample, while the shaded histogram represents leading muons with the same acceptance as the deep-inelastic sample; both refer to the normalized scale on the right.

Fig. 3. Combined kinematics of dimuon events, including polar angle difference $\Delta\theta$ [$=\theta_1 - \theta_2$], azimuthal angle difference (in the plane perpendicular to the beam axis) $\Delta\phi$ [$=\phi_1 - \phi_2$], apparent mass $M_{\mu\mu}$ [$=4E_1E_2 \sin^2(\Delta\theta/2)$], and inelasticity [$=(E_0 - E_1 - E_2)/E_0$]. The dashed curve represents the π/K decay and prompt muon backgrounds and the solid curve shows the elastic Bethe-Heitler contribution.

Fig. 4. Produced muon momentum (P_2) and its transverse momentum ($P_\perp$) relative to the virtual photon for dimuons. The upper (dash-dotted) curve represents the charm model prediction and the other curves are as described in Fig. 3.

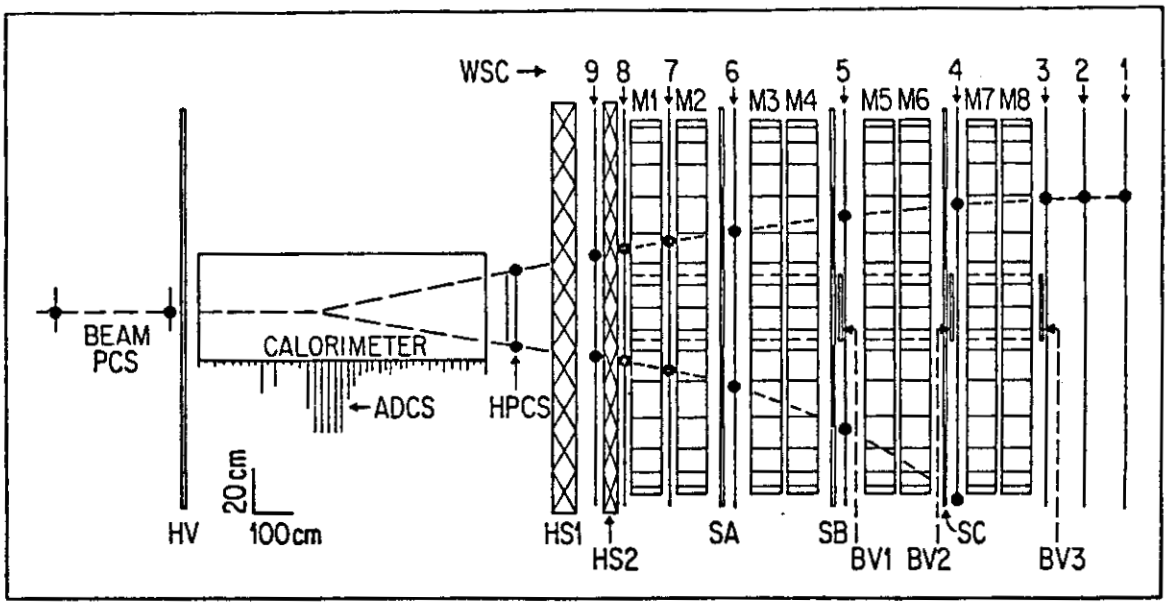

Figure 1

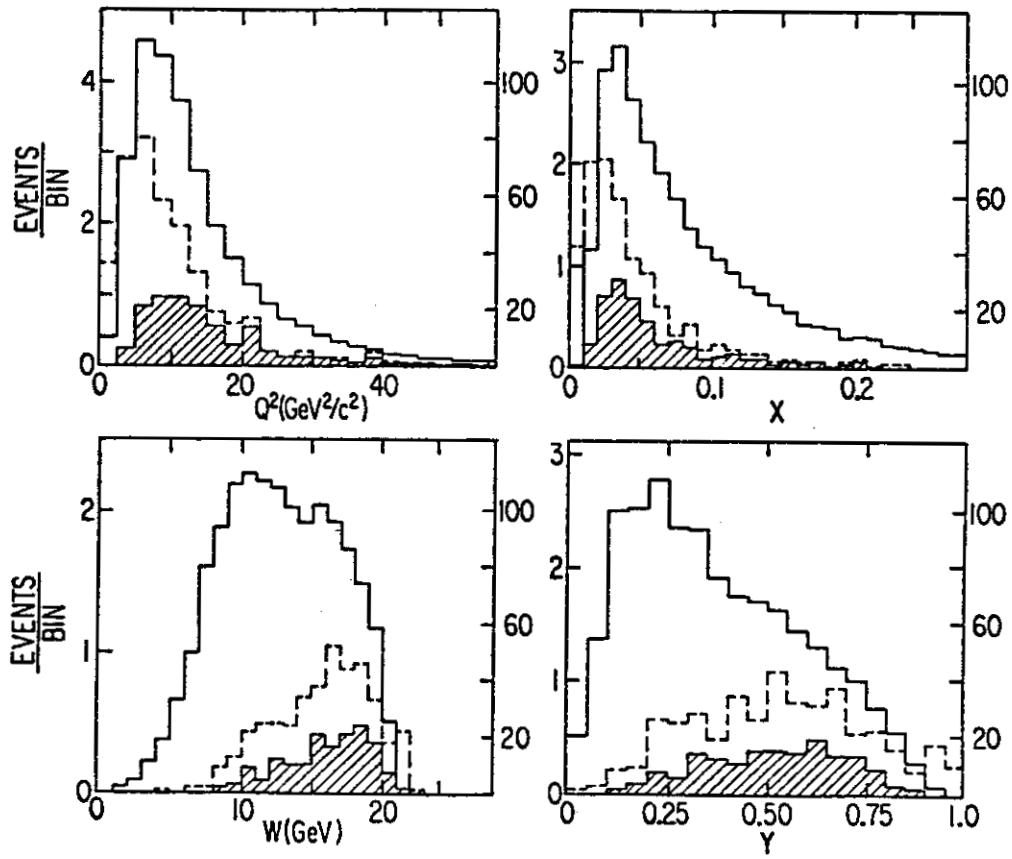

Fig. 2

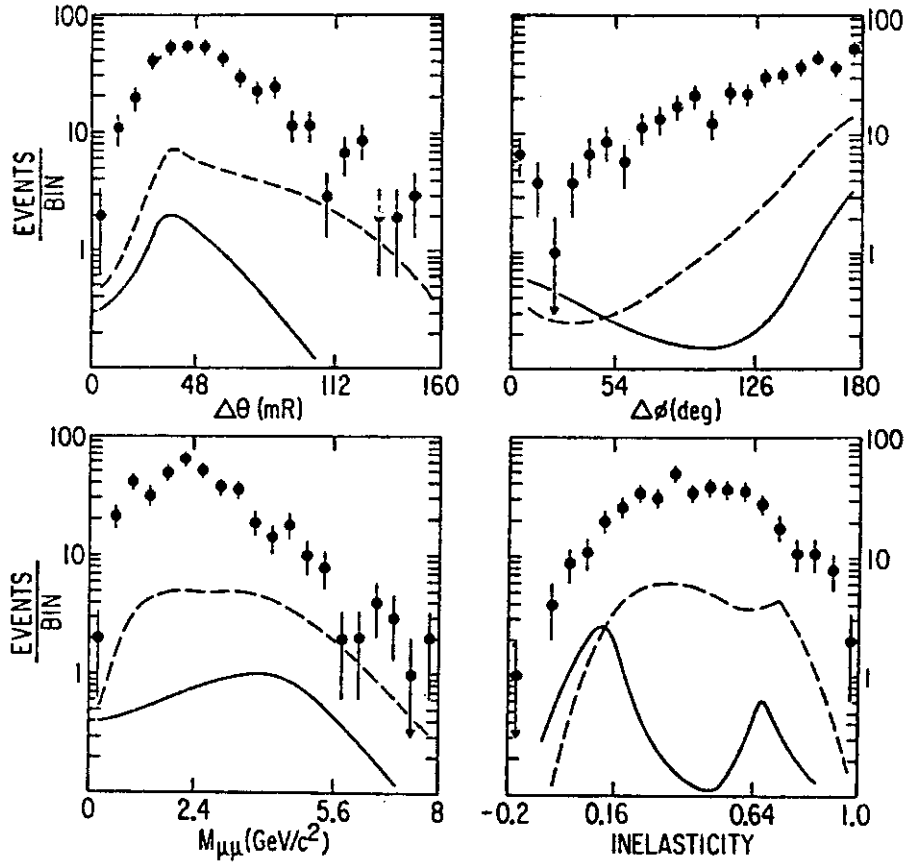

Figure 3

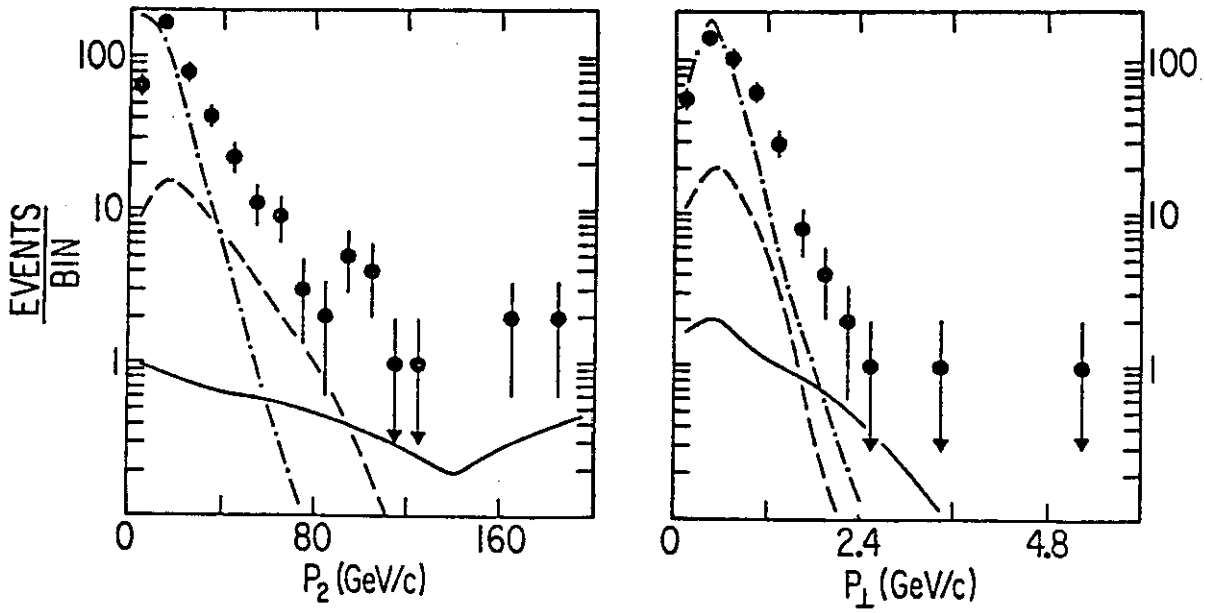

Figure 4